

# A Deterministic-Statistic Adventitia Detection in IVUS Images

Debora Gil<sup>1</sup>, Aura Hernandez<sup>1</sup>, Antoni Carol<sup>2</sup>, Oriol Rodriguez<sup>2</sup>,  
and Petia Radeva<sup>1</sup>

<sup>1</sup> Computer Vision Center, Universitat Autònoma de Barcelona,  
Bellaterra, Barcelona, Spain  
debora@cvc.uab.es  
<http://www.cvc.uab.es/debora/>

<sup>2</sup> Hospital Universitari Germans Trias i Pujol, Badalona, Spain

**Abstract.** Plaque analysis in IVUS planes needs accurate intima and adventitia models. Large variety in adventitia descriptors difficulties its detection and motivates using a classification strategy for selecting points on the structure. Whatever the set of descriptors used, the selection stage suffers from fake responses due to noise and uncompleted true curves. In order to smooth background noise while strengthening responses, we apply a restricted anisotropic filter that homogenizes grey levels along the image significant structures. Candidate points are extracted by means of a simple semi supervised adaptive classification of the filtered image response to edge and calcium detectors. The final model is obtained by interpolating the former line segments with an anisotropic contour closing technique based on functional extension principles.

## 1 Introduction

IVUS clinical interest feeds development of image processing techniques addressing detection of arterial structures [1], [2], such as lumen/intima segmentation or plaque characterization. However, although adventitia modelling is crucial for a reliable plaque quantification, the topic has been hardly approached. Regardless of low quality in IVUS images, adventitia detection adds the difficulty of a large variety of descriptors, which include image edges points of maximum variance (calcium) and tissue region segmentation. Deterministic strategies presented in previous works on adventitia detection exclusively basing on contour extraction are not reliable enough and need of either manual intervention [6] or laborious special treatment of sequences [7]. We argue that a robust adventitia segmenting algorithm should rely on learning strategies.

In this paper we address adventitia detection in two stages: a statistical extraction of points laying on the adventitia and a deterministic recovery of a closed model of the extracted points. At the first step, we define the quantities that best characterize the adventitia, that is, in the framework of classification, we should determine the optimal feature space of image descriptors. In such representation space, the adventitia should lie on a region isolated from other image

structures response, so that the problem of point selection reduces to determining the borders of such regions. Within this framework, there are several point selection strategies. On one side, we have statistical approaches [13] searching for a criterion to discriminate the target object representation in the feature space. On the other side, we apply a deterministic criterion of image smoothness to choose pixels achieving extreme values of the functions (filters) that determine the feature space. Still, even in this case, thresholding values should take into account the probability distribution of the image response to the describing filters. Therefore, whatever the decision criterion we adopt, the selection step nature is essentially statistical. Because the selected set of points is prone to be unconnected, contour completion is a compulsory second step. Usual techniques rely on deterministic principles: active models (parametric [4], geodesic [5] or region-based [14]) solve an energy minimizing problem and contour closing techniques [8] base on interpolation/functional extension methods.

The deterministic-statistical strategy for adventitia detection we propose is the following. For a better handling of the classifying problem, our feature space reduce to adventitia and calcium detectors, the latter to discard sectors with ambiguous information. In order to enhance significant structures while removing noise and texture response, we use a Restricted Anisotropic Diffusion [9] (RAD). For adventitia points selection, we search for the feature space partition (thresholds) achieving the best classification rate for a training set. For segment closing we suggest using an Anisotropic Contour Closing (ACC) [8] that bases on image local geometry for curve segment interpolation. Parametric B-spline snakes yield the final compact explicit model.

The topics are presented as follows. In Section 2 we thoroughly describe the way adventitia points are selected. Explanations about the main detection steps are given in Section 3. Section 4 is devoted to validation of the method and Section 5 to conclusions and further research.

## 2 A Deterministic Statistical Strategy

There are two main points in the segmentation process:

### 2.1 Statistical Selection of Adventitia Points

Since in an IVUS plane, the adventitia is a circular-wise structure (fig.1 (a)), we work in polar coordinates (see Section 3.1 for details). Let  $AdvPol(i, j)$  denote images in polar form (fig.1 (b)) with radius  $i = 1, \dots, R_{max}$ , and angle  $j = 1, \dots, 360$ . The selection stage summarizes in the next steps:

**Set of Descriptors.** The feature space for adventitia detection we propose reduces to the following two characteristics:

1. **Horizontal Edges ( $X$ )**

Since in the coordinate system chosen (fig. 1(b)), the adventitia layer is an horizontal dark line, horizontal edges constitute our main descriptor (see fig.

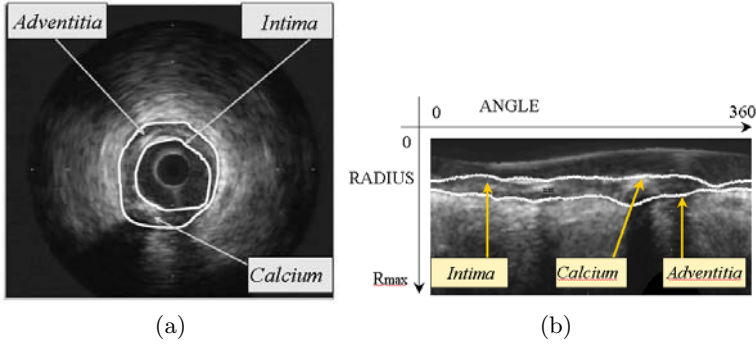


**Fig. 1.** IVUS images in cartesian (a) and polar (b) coordinates

2). Edges are computed by convolving the image with the  $y$ -partial derivative of a 2 dimensional gaussian kernel of variance  $\rho$ :

$$X = e_y(i, j) = g_y * AdvPol \quad \text{for} \quad g_y(x, y) = -\frac{y}{2\pi\rho^4} e^{-(x^2+y^2)/(2*\rho^2)}$$

Although intima and adventitia correspond to negative edges (fig.2), with a suitable (intima removing) strategy [10], this detector achieves optimal accuracy in the absence of calcium. Because at angles of calcium the adventitia does not appear and the detection is misled towards the intima, we discard those sectors. We base on calcium outstanding brightness to detect it by means of:

## 2. Radial Standard Deviation ( $Y$ )

Striking brightness corresponds to an outlier of the pixel gray value in the radial distribution. We measure it by means of the difference between the pixel gray value and the radial mean. For each pixel  $(i, j)$ , we define it as:

$$\sigma(i, j) = (AdvPol(i, j) - \nu(j))^2$$

where  $\nu(j)$  is the radial (i.e. column-wise) mean of the polar image:

$$\nu(j) = \frac{1}{R_{max}} \sum_{i=1}^{i=R_{max}} AdvPol(i, j)$$

Point clouds in fig. 2(b) show the feature space corresponding to the images in fig. 2(a). Adventitia corresponds to large negative  $X$  values and a small  $Y$  negative range, while calcium yields in the extreme positive values of the pair  $(X, Y)$ .

**Statistical Thresholding.** In a classification framework, determining the threshold values of the pair  $(X, Y)$  that characterize each structure reduces to finding a partition of the feature space separating adventitia and calcium from other vessel structures. Supervised techniques learn regions enclosing most of the

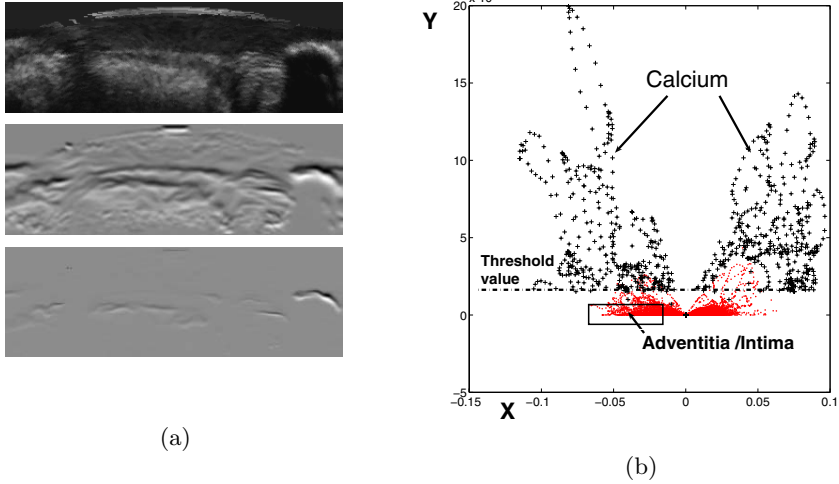


**Fig. 2.** Feature Space of Vessel Structures: X and Y responses, (a), and (X,Y) plane,(b)

training set, while ‘ad-hoc’ unsupervised clustering bases on the class instances structure given in a particular image. Although classical strategies exclusively follow either a supervised or an unsupervised approach, we adopt an adaptive criterion since mixed approaches [3] have proven to work better in IVUS images.

Because, in the feature space proposed, points of calcium correspond to extreme values, a supervised approach based on the Mahalanobis distance would work fine. However, by their spatial distribution, we have further reduced the decision criterion to choosing the threshold for Y values achieving the best compromise between true and fake classifications. On the other hand, if we consider all training images as a whole, adventitia points response presents a within class variability significant enough as to discard a fixed supervised criterion. By using a gaussian mixture [13] to model the training set density function, we have a misclassification error of 47.09% of fake detections for a test set. An unsupervised clustering is not sensible either since low dimensionality of the feature space introduces an overlapping between adventitia and other structures. What we propose is using an image sensitive classification based on searching for radial outliers in X negative values. That is, the thresholding value corresponds to the 5/6% percentile of the X values along each angle (columns in the polar image). This simple image adaptive criterion drops misclassification to 42.18% false positives corresponding to points on the intima layer.

## 2.2 A Restricted Diffusion Determined by Image Geometry

In order to smooth textures and strengthen response to the describing functions given in (2.1), we evolve the polar image under the following structure preserving filtering:

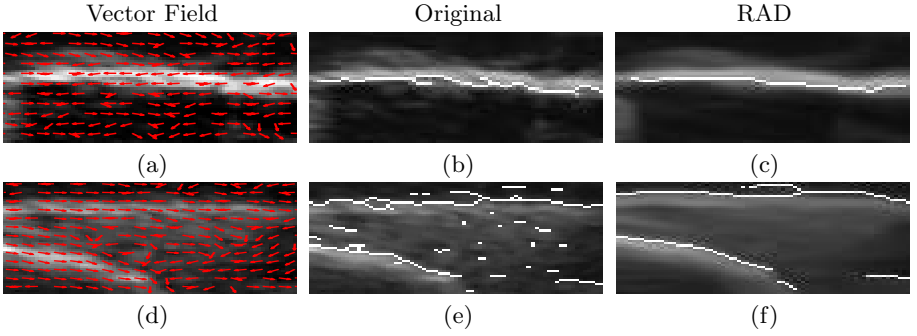


**Fig. 3.** RAD smoothing for calcium (1st row) and adventitia (2nd row)

**Restricted Anisotropic Diffusion (RAD).** Most filtering techniques based on image gray level modification [11] use the heat diffusion equation:

$$u_t(x, y, t) = \text{div}(J\nabla u)$$

The time dependent function  $u$  is the family of smoothed images and  $J$  is a 2-dimensional metric (i.e. an ellipse) that locally describes the way gray levels distribute. The diffusion tensor  $J$  is thoroughly described by means of its eigenvectors ( $\xi$ ,  $\eta = \xi^\perp$ ) and eigenvalues ( $\lambda_1$ ,  $\lambda_2$ ). If the latter ones are strictly positive, gray values spread on the whole image plane and the family  $u$  converges to a constant image. On the other side if we degenerate  $J$  (i.e. we admit null eigenvalues), then the final image [9] is a collection of curves of uniform gray level. Smoothing effects depend on the suitable choice of the eigenvector of positive eigenvalue. Let us consider a metric  $\tilde{J}$  with eigenvalues  $\lambda_1 = 1$  and  $\lambda_2 = 0$ , and  $\xi$  the eigenvector of minimum eigenvalue of the Structure Tensor [12]. If  $u_0$  is the image to be denoised, then the Restricted Heat Diffusion we suggest is given by:

$$u_t = \text{div}(\tilde{J}\nabla u) \text{ with } u(x, y, 0) = u_0(x, y) \quad (1)$$

Figure 3 illustrates the way restricted diffusion works. Around the image significant structures (calcium in fig.3(a)),  $\xi$  represents the tangent space to a closed model of such structures. Meanwhile at noisy areas (textured tissue in fig.3(d)), it is an irregular vector with random orientation. The result is that gray levels homogenize along image regular level sets and solutions to (1) converge to a smooth image that enhances the main features of the original image, in the sense that their response to standard detectors is uniform. Figure 3 shows the improvement of calcium (first row) and edges (second row) responses after applying RAD. Background spurious edges due to noise in fig.3(e) have been removed, in a similar fashion a gaussian smoothing would do, while edges corresponding to the vessel adventitia and calcium are continuous closed curves in the RAD images of fig.3(c),(f).

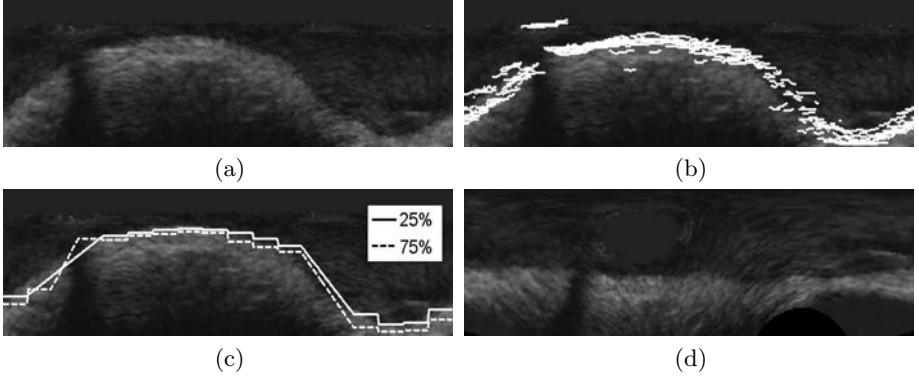


**Fig. 4.** Straighten adventitia layer procedure

**Anisotropic Contour Closing (ACC).** Heat diffusion has also the property of smoothly extending a function defined on a curve in the plane, provided that boundary conditions are changed to Dirichlet [15]. By using restricted heat operators this property can be used to complete unconnected contours [8] as follows. Let  $\gamma$  be the set of points to connect,  $\chi_\gamma$  its characteristic function (a mask) and define  $\tilde{J}$  as in RAD, then the extension process given by:

$$u_t = \operatorname{div}(\tilde{J}\nabla u) \text{ with } u|_\gamma = u_0 \quad (2)$$

converges to a closed model of  $\gamma$ . Intuitively, we are integrating the vector field  $\xi$ , that is, we are interpolating the unconnected curve segments along it. This fact not only ensures convergence to a closed model, but also yields closures more accurate than other interpolating techniques (such as geodesic snakes [5]).

### 3 Adventitia Modelling Steps

The characterization strategy of Section 2 serves to model the adventitia layer in the following three step procedure.

#### 3.1 Polar Coordinates Origin

Polar coordinates with a fixed origin at the center of the cartesian image present two main artifacts produced by cardiac movement and the artery geometry. In cartesian coordinates, heart movement induces a translation followed by a rotation. This motion converts into an angular translation (rotation) and a radial dynamic wave (translation). The latter is a main artifact for the set of descriptors given in Section 2.1 and it is removed by taking as origin of coordinates the mass center of the image (fig. 4(a)). In such coordinates, the adventitia still presents a slight static wavy shape because image mass centers do not coincide with geometric centers. We correct this deformation by means of a set of

points extracted using the strategy described in Section 2. The impact of noise is minimized by considering the average of the energy  $e_y$  in the sequence temporal direction (fig. 4(b)). In order to endow further continuity to the extracted edges, we use the statistical distribution of their position in angular sectors of the cartesian image. For each sector we only consider edge points within the central percentile computed for a given number of frames (fig. 4(c)). The mass center of the cartesian transform of the former radial values serves as geometric center of the adventitia layer and is the origin of our polar transform. Fig. 4 (d) shows the final polar coordinates.

### 3.2 Adventitia Selection

The classification of the filtered images given by RAD yields a calcium and adventitia masks. Small structures in the adventitia image are removed by applying a length filtering, so that only segments of length above the 75% percentile are kept. In order to remove intima points, we consider that an edge connected component is on the adventitia layer if it corresponds to an edge of maximum radius in a longitudinal cut of the sequence.

### 3.3 Adventitia Closing

We split interpolation of the selected curve segments into computation of an implicit closed representation and explicit encoding with parametric B-splines.

For adventitia completion we will use ACC with the Structure Tensor defining the vector  $\xi$  computed over the edge map used in the selection step. In order to obtain models as accurate as possible, the vector  $\xi$  is weighted by the coherence of the Structure Tensor:

$$coh = \frac{(\lambda_1 + \lambda_2)^2}{(\lambda_1 - \lambda_2)^2}$$

where  $\lambda_1 \geq \lambda_2$  are the eigenvalues of the tensor. At regions where  $\xi$  is a continuous vector,  $\lambda_2$  is closed to zero, so  $coh$  is maximum, meanwhile, at noisy areas, since  $\xi$  is randomly oriented,  $\lambda_1$  compares to  $\lambda_2$  and  $coh \sim 0$ . In this manner we avoid wrong interpolations at side branches and sensor shadows sectors.

The final model discards angles presenting response to calcium and uses B-splines to smoothly interpolate the adventitia at side branches and calcium sectors.

## 4 Results

Objective quantitative validation of the method has been based on the following assessment protocol. A total number of 3300 frames extracted from 9 different patients, including 4 sequences with calcium, have been analyzed. The measures used to quantify accuracy of the automated detections are the mean and maximum distance error (in *mm*) and area differences (in percentages) between our model and an expert manual segmentation. The sequences have been manually segmented by 3 different physicians every 10 frames in order to analyze inter-

observer variation. Figure 5 shows adventitia snake models for soft plaque (fig.5 (a), (d)), calcium (fig.5 (b), (e)) and at a side branch (fig.5 (c), (f)).

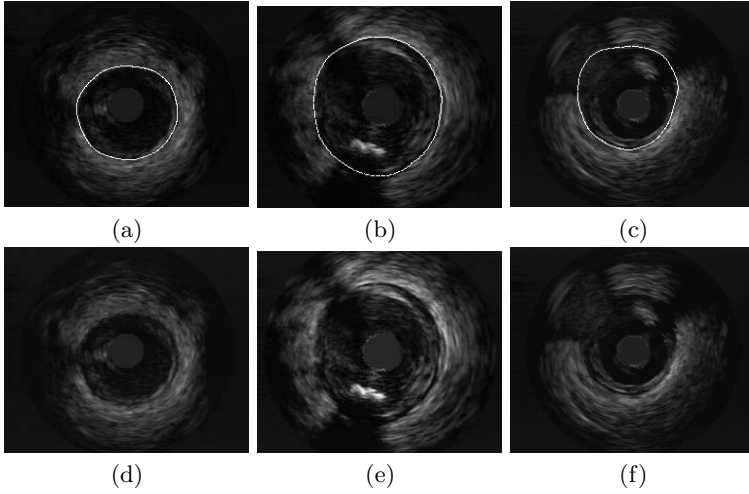


**Fig. 5.** Segmentations (a), (b), (c) for different plaque (d), (e) and at a side branch (f)

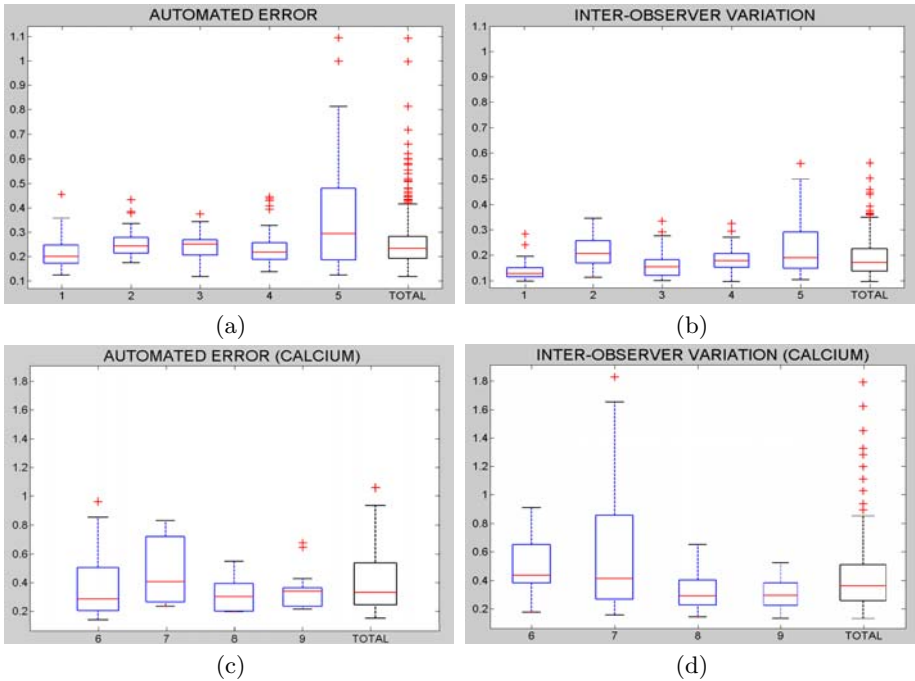


**Fig. 6.** Whisker Boxes for Automated Error and Inter-Observer Variation

## 4.1 Statistical Measurements

Figure 6 shows whisker boxes for mean distance absolute errors and inter-observer variations for soft plaque (1st row) and calcium segments (2nd row). They summarize the statistics for each patient and for the total population at the last box on the right. An analysis of the whisker boxes reflects robustness of segmentations: the smaller the boxes are, the more reliable the method is. First note that, lack of reliable information at large angular sectors, significantly increases errors variability in calcified segments (fig.6(c), (d)), especially for manual segmentations, due to the subjectivity of manually traced curves. Still, our strategy is highly stable as, in most cases, graphics present a smaller variability than manual models. Only subject 5 has a large variability, but, comparing, with manual errors (fig.6(b)), we observe that this subject is also the one presenting the largest box. Average relative and absolute errors in distances and percentage of area difference for the total number of patients (excluding the outlier case 5) are summarized in table 1. Mean distances compare to inter-observer variability and maximums, although above it, are less than 1% of the vessel radius.

**Table 1.** Statistics on Errors

	Max. Dist. (mm)		Mean Dist. (mm)		Area Dif. (%)
	Abs. Error	Rel. Error (%)	Abs. Error	Rel. Error (%)	
INT-OBS.	$0.560 \pm 0.326$	$0.5 \pm 0.28$	$0.284 \pm 0.222$	$0.247 \pm 0.203$	$8.294 \pm 3.914$
AUT.	$0.655 \pm 0.349$	$0.619 \pm 0.4$	$0.273 \pm 0.131$	$0.243 \pm 0.120$	$10.287 \pm 4.369$

## 5 Conclusions

Using an integrated approach of statistic classification and anisotropic filtering to detect the adventitia layer presented in this paper is a new trend in medical imaging with a straightforward clinical application to plaque area and vessel diameter measurements. The strategy proposed combines statistical classification and deterministic energy based techniques into a two step algorithm. On a first stage, a set of adventitia and calcium descriptors are proposed as a feature space. A supervised analysis of such 2-dimensional space serves to determine those regions enclosing target points. Feature extraction is optimized by applying a response regulating restricted diffusion operator to polar IVUS images. The second step involves computation of a closed model of the selected curve segments. An anisotropic contour closing is used for obtaining an implicit representation that captures all geometric features.

Statistics show that automated errors are comparable to inter-observer variability as far as adventitia can be detected by means of the proposed descriptors. Since accuracy exclusively relies on such features, our future research will focus on adding some a priori knowledge on vessel tissue.

## References

1. McInerney, T., Terzopoulos, D.: Deformable models in medical images analysis: a survey, *Medical Image Analysis*, **1** (1996) 91–108
2. Zhang, X., Sonka, M.: Tissue characterization in intravascular ultrasound images, *IEEE Trans. on Medical Imaging*, **17** (1998) 889–899
3. Pujol, O., Radeva, P.: Supervised Texture classification for Intravascular Tissue Characterization, *Handbook of Medical Imaging*, Kluwer Academic/Plenum Pub. (2004)
4. Kass, A., Witkin, A. and Terzopoulos, D.: Snakes: Active Contour Models, *Int. Journal of Computer Vision*, **1** (1987) 321–331
5. Caselles, V., Kimmel, R., Sapiro, G.: Geodesic Active Contours, *Int. J. Comp. Vision*, **22** (1) (1997) 61–79
6. Klingensmith, J.D., Shekhar, R., Vince, D.G.: Evaluation of three-dimensional segmentation algorithms for the identification of luminal and Medial-adventitial borders in intravascular ultrasound, *IEEE Trans. on Med. Imag.*, **19**(10), (2000) 996–1011
7. von Birgelen, C., de Vrey, E. A., Mintz, G. S., Nicosia, A., Bruining, N., Li, W., Slager, C. J., Roelandt, J. R. T. C., Serruys, P. W. and de Feyter, P. J.: ECG-gated three-dimensional intravascular ultrasound: Feasibility and reproducibility of the automated analysis of coronary lumen and atherosclerotic plaque dimensions in humans, *Circulation* **96**, (1997) 2944–2952
8. Gil, D., Radeva, P.: Extending Anisotropic Operators to Recover Smooth Shapes, *Comp. Vis. Imag. Unders.*, (in press)
9. Gil, D.: Geometric Differential Operators for Shape Modelling, PhD Tesis, Universitat Autònoma de Barcelona, (2004) (available at <http://www.cvc.uab.es/debora/>)
10. Hernandez, A., Gil, D., Radeva, P., E. Nofrerias,: Anisotropic Processing of Image Structures for Adventitia Detection in IVUS Images, *Proc CiC*, (2004)
11. Weickert, J.: A Review of Nonlinear Diffusion Filtering, *Scale-Space Theory in Computer Vision*, Lecture Notes in Comp. Science, Springer-Verlag, (1997)
12. Jähne, B.: Spatio-temporal image processing, *Lect. Notes in Comp. Science*, Springer, (1993)
13. Duda, R., Hart, P.: *Pattern Classification*, Wiley-Interscience, (2001)
14. Paragios, N., Deriche, R.: Geodesic Active Contours for Supervised Texture Segmentation, *Proc. of Comp. Vis. and Pat. Rec.* **2**, (1999), 422–427
15. Evans, L.C.: *Partial Differential Equations*, Berkeley Math. Lect. Notes (1993)